



## Revealing mercury species-specific transfer and toxicity mechanisms in placental trophoblasts

Vivien Michaelis<sup>a,\*</sup>, Laura Klemens<sup>a</sup>, Alicia Thiel<sup>a</sup>, Anna Gremme<sup>a</sup>, Maria Schwarz<sup>b,c</sup>, Anna P. Kipp<sup>b,c</sup>, Hans Zischka<sup>d,e</sup>

<sup>a</sup> Food Chemistry with Focus on Toxicology, Faculty of Mathematics and Natural Sciences, University of Wuppertal, Germany

<sup>b</sup> Department of Nutritional Physiology, Institute for Nutritional Sciences, Friedrich-Schiller University Jena, Jena, Germany

<sup>c</sup> TraceAge-DFG Research Unit on Interactions of Essential Trace Elements in Healthy and Diseased Elderly (FOR 2558), Berlin-Potsdam-Jena-Wuppertal, Germany

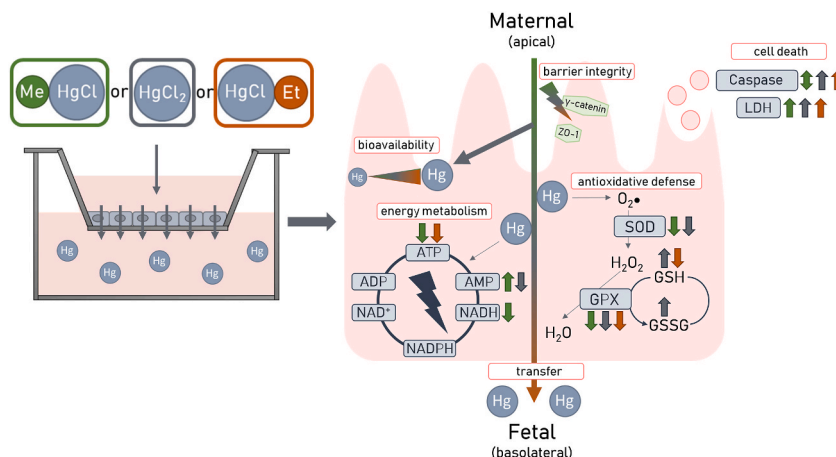
<sup>d</sup> Institute of Molecular Toxicology and Pharmacology, Helmholtz Center Munich, German Research Center for Environmental Health, Neuherberg, Germany

<sup>e</sup> Institute of Toxicology and Environmental Hygiene, School of Medicine and Health, Technical University Munich, Munich, Germany

### HIGHLIGHTS

- Hg species-specific transfer mechanism and bioavailability in placental trophoblasts.
- Hg-induced impairment of barrier integrity by disruption of tight junction proteins ZO-1 and  $\gamma$ -catenin.
- Reduction in SOD and GPX activity upon Hg exposure.
- Perturbation of the energy metabolism and antioxidant defense by means of GSH/GSSG.

### GRAPHICAL ABSTRACT



### ARTICLE INFO

Handling editor: Milena Horvat

#### Keywords:

Mercury  
Placenta  
Barrier integrity  
Oxidative stress  
Cellular metabolism

### ABSTRACT

Environmental mercury (Hg) follows a biogeochemical cycle resulting in a variety of Hg species. Therefore, human exposure to the three Hg species inorganic Hg via crops and air, methyl Hg through fish consumption and ethyl Hg due to the use as antiseptic agent in medical applications is a rising concern. Especially pregnant women and their developing fetus present a vulnerable population. However, little is known about its transfer and toxicity in placental barrier building cells. Here, Hg species-specific transfer and toxicity in placental trophoblasts, which are the main cell type involved in nutrient transfer, were investigated by using the established BeWo b30 *in vitro* model. The transfer of inorganic Hg was much lower compared to the organic Hg species and all three species were able to perturb barrier integrity. This was accompanied by a less pronounced cytotoxicity

\* Corresponding author. Food Chemistry with Focus on Toxicology, Faculty of Mathematics and Natural Sciences, University of Wuppertal, Gaußstraße 20, 42119, Wuppertal, Germany.

E-mail address: [michaelis@uni-wuppertal.de](mailto:michaelis@uni-wuppertal.de) (V. Michaelis).

<https://doi.org/10.1016/j.chemosphere.2024.143870>

Received 10 July 2024; Received in revised form 26 November 2024; Accepted 29 November 2024

Available online 13 December 2024

0045-6535/© 2024 The Authors. Published by Elsevier Ltd. This is an open access article under the CC BY license (<http://creativecommons.org/licenses/by/4.0/>).

of  $\text{HgCl}_2$  compared to the two organic species. The energy charge value indicated an increase for inorganic Hg and a decrease for organic Hg compounds. Regarding antioxidative defense, inorganic Hg elevated GSSG levels, while organic Hg decreased GSH. Activity of antioxidative defense related enzymes showed a decrease upon Hg species treatment and all three species induced both apoptotic and necrotic cell death.

## 1. Introduction

Mercury (Hg) is a persistent pollutant which occurs naturally due to volcanic or geothermal activities among others (Pirrone et al., 2010). The enrichment of Hg in the atmosphere however is driven by anthropogenic activities like combusting of fossil fuels or industrial processes increasing the airborne Hg levels three-fold. Once in the environment it is transformed into Hg species with different oxidation states and chemical properties. In the environment, inorganic Hg is present, while organic forms like methyl mercury (MeHg) are formed due to a biogeochemical cycle where Hg is methylated by sulfate-reducing bacteria in the aquatic habitat. Biomagnification and bioaccumulation processes allow MeHg to enter the aquatic food chain, reaching high levels predominantly in predatory fish (Broczka et al., 2024; Dorea et al., 2006; Novo et al., 2021). Recent findings of a total diet study by the German Federal Institute of Risk Assessment confirmed that high amounts of Hg are still a concern in fish, which are consumed by the general population (Fechner et al., 2022). Next to Hg as an environmental pollutant it is still used in the medical setting as thimerosal in meningococcal and tetanus-toxoid vaccines in the developing world because of its preserving, antiseptic, and antifungal properties. It rapidly degrades to ethyl mercury (EtHg), another organic Hg species (Dorea et al., 2013). By reasons of its widespread occurrence, which is still increasing since the start of the industrialization, humans can be exposed environmentally and occupationally to elemental and inorganic Hg, while the enrichment of the organic MeHg in fish represent the nutritional exposure route of Hg (Park and Zheng, 2012; Yang et al., 2020). Due to the accumulation in the environment, Hg from contaminated soils can be taken up through the roots of different crops (Alissa and Ferns, 2011; Gao and Wang, 2018).

Inorganic Hg and organic Hg species are highly toxic but follow different toxicological profiles. In humans the main target of inorganic Hg-induced toxicity is the kidney and especially the epithelial cells of the proximal tubule (Oliveira et al., 2015; Zalups, 2000). Compared to inorganic  $\text{HgCl}_2$ , organic Hg species like MeHg readily cross the blood brain barrier (Lohren et al., 2016). MeHg is prone to accumulate in the cerebellum leading to the loss of cerebellar glutamatergic granule cells. This manifests in clinical symptoms such as ataxia and impairment of the locomotion (Albers et al., 2020; Novo et al., 2021). At cellular level MeHg exposure correlates with the induction of oxidative stress, increased excitotoxicity, DNA damage, mitochondrial damage, and calcium dyshomeostasis (Farina et al., 2011; Novo et al., 2021). These neurotoxic mechanisms are deleterious especially for the developing brain. Prenatal and early postnatal exposure to MeHg have been shown to impair the structure and functions of the central nervous system, i.e. loss of neurons and glial cells induced by inadequate differentiation, and growth. This in turn might lead to behavioral abnormalities later in life such as reduced motor activity, or decreased learning ability (Björklund et al., 2007; Li et al., 2021; Paletz et al., 2006). Therefore, the WHO nominated Hg among others as ten key chemicals with public health concern (WHO, 2017). The European Food Safety Authority (EFSA) and the Joint FAO/WHO Expert Committee on Food Additives (JECFA) postulated a tolerable weekly intake (TWI) of 4  $\mu\text{g}/\text{kg}$  body weight for inorganic Hg and a provisional tolerable weekly intake of 1.6  $\mu\text{g}/\text{kg}$  bodyweight for MeHg, which was reevaluated to a TWI of 1.3  $\mu\text{g}/\text{kg}$  body weight due to new epidemiological data. In case of high fish consumption this TWI may be exceeded up to six-fold (EFSA, 2012; FAO/WHO, 2007, 2011). In the human body inorganic Hg and organic Hg have a half-life from 60 up to 120 days, respectively (Park and Zheng,

2012; Rand and Caito, 2019).

Cellular structures like the placental barrier are limiting the excessive transfer of pollutants and xenobiotics (Tetro et al., 2018). However, the affinity of Hg to thiol-containing enzymes and proteins characterizes the hazardous nature for the developing fetus. Hg binding to cysteine for example, is in a chemical mimicry with L-methionine, an essential amino acid (Hoffmeyer et al., 2006). Therefore, Hg is transported readily across placental structures by amino acid transporters. In literature, the transport of MeHg across the placental barrier has been identified, while some studies suggest absent transport of inorganic Hg because of the missing lipophilic character compared to organic Hg species (Balthasar et al., 2017; Park and Zheng, 2012). Nevertheless, a study by Oliveira et al. showed that, upon  $\text{HgCl}_2$  administration (0.5 or 2.5  $\mu\text{mol}/\text{kg}$ ) to pregnant wistar rats Hg accumulated rapidly in placental tissues and fetal organs (Oliveira et al., 2015). A cohort study identified positive correlation between nutritional Hg exposure through fish and vegetables and Hg amount found in placental tissues (Molina-Mesa et al., 2022). However, little is known about Hg effects on placental structures. In particular, there is a gap of knowledge on adverse effects of different Hg species in placental trophoblasts, which are key players in the transport of nutrients from the mother to the fetus (Ganapathy et al., 2021; Li et al., 2021). Therefore, this study aims to elucidate species-specific transfer kinetics of inorganic Hg and two different organic Hg species, namely MeHg and EtHg, all of which are potential toxicants for pregnant woman regarding environmental, occupational or nutritive exposure. For this we utilized the *in vitro* BeWo b30 transwell system, which resembles characteristics of the trophoblast layer of the placental barrier. Furthermore, investigation of the effects of the Hg species on barrier integrity as well as the energy- and glutathione metabolism and antioxidative defense system will identify potential modes of toxicity.

## 2. Materials and methods

### 2.1. Cultivation of BeWo b30 cells

BeWo b30 cells are derived from a gestational chorioncarcinoma and were cultured as described previously (Michaelis et al., 2022). Briefly, BeWo b30 cell culture was maintained using Ham's F12-K medium (Thermo Fisher Scientific (Gibco), Schwerte, Germany), supplemented with 1 % fetal calf serum (FCS superior, Sigma Aldrich, Steinheim, Germany), 1 % penicillin/streptomycin (Sigma Aldrich), and 2 mM L-glutamine (Sigma Aldrich). Cells were sub-cultured twice a week with 0.05 % trypsin-EDTA solution (Sigma Aldrich) and cultured in a humidified incubator at 37 °C with 5 %  $\text{CO}_2$ . To maintain a reproducible *in vitro* system, BeWo b30 cells were sub-cultured only 5 times. For transfer and toxicity tests, cells were seeded in endothelial growth medium MV supplemented with 1 vial SupplementMix according to the manufacturer's manual (PromoCell, Heidelberg, Germany), and 1 % penicillin/streptomycin.

### 2.2. Mercury dosage regime and cytotoxicity measurement

Stock solutions of  $\text{HgCl}_2$  (20 mM) and MeHgCl (5 mM), ( $\text{HgCl}_2$ , 99.9995 % Hg,  $\text{CH}_3\text{HgCl}$ , ABCR GmbH & Co. KG, Karlsruhe, Germany) were prepared freshly prior to the experiment in sterile purified water (18  $\text{M}\Omega\cdot\text{cm}$ ) to avoid decomposition. A stock solution of EtHgCl (5 mM,  $\text{C}_2\text{H}_5\text{HgCl}$ , ABCR GmbH & Co. KG, Karlsruhe, Germany) was prepared in MeOH shortly before the experiment due to preceding reasons. In order to distinguish MeOH induced effects from those induced by EtHgCl we

included a vehicle control. For the determination of cytotoxicity, HgCl<sub>2</sub> was applied in doses ranging from 0 to 400 μM, MeHg from 0 to 50 μM, and EtHg from 0 to 15 μM. Further cytotoxicity was assessed using the Hoechst assay as published before (Michaelis et al., 2023). For all other experiments, concentration ranges were chosen depicting the sub-toxic to near toxic region. Therefore, concentrations of 10–50 μM HgCl<sub>2</sub>, 0.5–5.0 μM MeHgCl, and 0.75–1.5 μM EtHgCl were incubated for an incubation time of 24 h. For investigating Hg accumulation sites concentrations were used that did not reach the cytotoxic range. Using concentrations higher than those already mentioned led to a disturbed BeWo b30 cell barrier and were excluded from this study. Unless otherwise stated, vehicle control (MeOH) showed no significant changes compared to untreated control and is therefore excluded in the graphs.

### 2.3. Transfer of mercury species across the BeWo b30 cell layer

Transfer experiments were realized as described previously (Michaelis et al., 2022). Briefly  $8.5 \times 10^4 - 1.5 \times 10^5$  cells were seeded on the apical side of microporous inserts (Transwells® with a polycarbonate membrane, 0.4 μm pore size, 1.12 cm<sup>2</sup> growth area, Corning Life Sciences, Amsterdam, Netherlands) coated with 50 μg/mL human placental collagen (Sigma Aldrich). Three days after seeding medium was changed 2 h before Hg treatment. Barrier tightness was monitored during the time of incubation measuring the transepithelial electrical resistance (TEER) using the cellZscope® device (nanoAnalytics, Münster, Germany). Samples to determine transferred Hg content were taken from the apical and basolateral compartment, 2, 6 and 24 h after treatment. To quantify Hg content in cells grown on inserts, the membrane was cut out with a scalpel and washed with ice-cold PBS to remove remaining medium and Hg. For cell lysis, cells were digested in a lysis buffer containing 1 mM TRIS, 0.1 M NaCl, 1 mM EDTA disodium salt, and 0.1 % Triton™ X-100.

### 2.4. ICP-OES method to determine mercury concentrations in medium and cell extracts

Determination of Hg in medium and cell extracts was realized by using inductively coupled plasma-optical emission spectroscopy (ICP-OES) calibrated externally and published recently (Friedrich et al., 2024). Due to difficulties of Hg plastic adherence and memory effect during the measurement, calibration as well as sample solutions were diluted in 0.2 % L-cysteine prepared with a mixture of 2 % nitric acid (HNO<sub>3</sub>; Suprapur®, Supelco, Sigma Aldrich) and 0.1 % hydrochloric acid (HCl; Suprapur®, Supelco, Sigma Aldrich). ICP-OES measurements were validated using certified reference material BCR® (single cell protein, Institute for Reference Materials and Measurement of the European Commission, Geel, Belgium), which was acid-assisted digested beforehand, and SRM®-1643f (Natural Water, National Institute of Standards & Technology, Gaithersburg, USA) both spiked with Hg standard solution (1000 mg/L in 10 % HNO<sub>3</sub>, Carl Roth) in the low (10 μg/L) and high (100 μg/L) concentration range. Measurement parameters are provided in Table 1. The cellular Hg concentration was normalized to protein amount determined by BCA assay and medium concentrations were normalized to the applied dose.

### 2.5. Immunocytochemical staining of tight junction proteins

The immunocytochemical staining of tight junction proteins was performed as described in Aengenheister et al., (2018). For this, cells were fixed using 4 % PFA and 0.2 % Triton™ X-100 for 10 min at room temperature (RT). After washing with PBS, inserts were blocked with 5 % goat serum in PBS (Invitrogen, Thermo Fisher Scientific) for 30 min at 37 °C. Afterward, a 1:500 dilution of mouse anti-(γ)-catenin (BD Biosciences, Heidelberg, Germany) in 0.5 % BSA/PBS was applied for 1 h at RT. For zonula occludens 1 (ZO-1) staining, a 1:250 dilution of rabbit anti-ZO-1 in 0.5 % BSA/PBS was incubated for 30 min at 37 °C. After an

**Table 1**

Method parameters ICP-OES measurement of Hg.

Parameter	Working conditions
Plasma power [W]	1500
Cooling gas flow [L/min]	10
Auxiliary gas flow [L/min]	0.2
Nebulizer flow [L/min]	0.7
Nebulizer type	MicroMist®
Torch alignment	Axial
Sample flow (mL/min)	1
Flush time	20 s (1.5 mL/min)
Element wavelengths [nm]	Hg (I): 253.652 Mn (II): 257.611 Fe (II): 259.940 Cu (I): 327.393 Zn (I): 213.856 Y(II): 371.029 (internal standard)

additional washing step with PBS, ZO-1 treated cell layers were blocked additionally with 3 % BSA/PBS for 20 min at RT. An A488 goat anti mouse (diluted 1:400 in 0.5 % BSA/PBS), and A488 mouse anti-rabbit (diluted 1:1000 in 0.5 % BSA/PBS) (Invitrogen, Thermo Fisher Scientific) antibody were used for 2nd antibody staining for 1 h at RT or 30 min at 37 °C, respectively. Before mounting, the nucleus was stained using 1 % Bisbenzimidazole H 33258 (Hoechst, Calbiochem, Sigma Aldrich) in MeOH for 30 s at RT. To ensure an even surface, whole insert membranes were embedded in Mowiol 4–88 (Sigma Aldrich) at 40 °C overnight. Immunocytochemical analysis was performed with inserts incubated with the highest Hg concentrations. Immunostaining was captured with a Leica DMB6 fluorescence microscope (Leica Camera AG, Wetzlar, Germany) using L5 and 405 filters and 60-fold magnification objects. Images were processed using the Leica Thunder to extract overlaying fluorescence intensity of the mounting medium.

### 2.6. LC-DAD measurement of energy-related nucleotides

For the determination of energy-related nucleotides 31,000 cells/cm<sup>2</sup> were seeded on culture dishes and incubated with the respective Hg species for 24 h. The cell number and volume were quantified using an automated cell counter (CASY®TTC, OMNI Life Science GmbH, Bremen, Germany). Cells have to be prepared immediately due to the instability of ATP. For this, 20 PTFE beads were added to each sample. After adding 150 μL 0.5 M KOH, cell pellets were homogenized via bead ruptor (biolab products, Bebensee, Germany) for 40 s at high intensity. Exactly after 60 s of adding KOH, pellets were neutralized using 30 μL of 10 % phosphoric acid (H<sub>3</sub>PO<sub>4</sub>). The samples were centrifuged at 18,620×g, 4 °C for 30 min. The supernatant was directly used for LC-DAD analysis. Energy-related nucleotides were quantified by external calibration and normalized to cell volume (Bornhorst et al., 2012). To indicate potential changes in the overall energy metabolism the energy charge value (AEC) was determined using the following equation:

$$AEC = \frac{ATP \text{ levels} + (0.5 * ADP \text{ levels})}{\text{total adenosine nucleotides}}$$

### 2.7. LC-MS/MS analysis of GSH and GSSG levels

Reduced glutathione (GSH) and oxidized glutathione (GSSG) levels were determined simultaneously by LC-MS/MS according to Thiel et al. (2023). To avoid oxidation of GSH during sample preparation N-ethylmaleimide (NEM, ≥98 %, Merck (Sigma Aldrich)) was used to reduce free thiol groups of present GSH. For sample preparation cell pellets were pelleted and resuspended in 300 μL extraction buffer (16 mM KH<sub>2</sub>PO<sub>4</sub>, 84 mM K<sub>2</sub>HPO<sub>4</sub>, 8.8 mM EDTA, 2 mM NEM, 1 % Triton™ X-100, 0.6 % sulfosalicylic acid), and homogenized using four bead rupturing cycles (20 s, high intensity). After centrifugation for 10 min at 18,620×g, 4 °C the supernatant was transferred onto a SpinX® filter

(0.22  $\mu\text{m}$  pore size, Corning Life Sciences) and centrifuged for 5 min with the same parameters used before. The eluate can be used for HPLC-MS/MS analysis. GSH and GSSG levels were quantified by external calibration and normalized to cell volume.

### 2.8. Determination of SOD activity levels

Total SOD activity was assessed by using the SOD Assay Kit-WST (Dojindo Molecular Technologies Inc., Kumamoto, Japan) based on the reduction of WST-1 by superoxide anions forming a formazan dye which absorbance can be measured at 450 nm using a microplate reader. Assay preparation was done according to the manufacturer's protocol. For sample preparation cells were pelletized and were washed using the included dilution buffer. After aspiration of the supernatant, fresh dilution buffer was added followed by 2 freeze/thaw cycles (1 min liquid nitrogen, 1 min 37 °C water bath) and two bead rupturing cycles (20 s, high intensity). The cell suspension was centrifuged at 10,000 $\times$ g at 4 °C for 20 min. The supernatant was used for SOD activity analysis and evaluated against a SOD concentration curve (SOD from bovine erythrocytes, Sigma Aldrich). Data were normalized to the cell volume.

### 2.9. Determination of GPX activity levels

GPX activity was determined as described previously (Schwarz et al., 2023). Briefly, cells were pelletized and the cell pellet was resuspended in homogenization buffer (100 mM Tris, 300 mM KCl, 0.1 % Triton-X-100). After two bead rupturing cycles (20 s, high intensity) the cell lysates were centrifuged at 14,000 $\times$ g at 4 °C for 15 min. After a dilution of 1:5, samples and a reaction mix consisting of Tris/EDTA buffer (100 mM Tris, 5 mM EDTA, 1 mM NaN<sub>3</sub>), 10 % Triton™ X-100, 20 mM NADPH, 300 mM GSH, and 14.1 U/mL glutathione reductase were transferred into a 96 Well. After an incubation time of 15 min at 37 °C and addition of 0.003 % H<sub>2</sub>O<sub>2</sub> as a substrate, NADPH consumption was measured using a microplate reader at 340 nm.

### 2.10. Caspase-3 and lactate dehydrogenase release assay

Caspase-3 activity and lactate dehydrogenase release was determined as described previously and normalized to protein amount assessed by BCA assay (Michaelis et al., 2023; Smith et al., 1985).

### 2.11. Statistical analysis

Statistical analysis was performed using GraphPad Prism 10 Software (GraphPad Software, La Jolla, CA, USA). Unless otherwise stated, data is shown as mean  $\pm$  SD. Significance values obtained by Ordinary One-Way ANOVA or unpaired student's t-test are depicted as followed: \*p < 0.05, \*\*p < 0.01, \*\*\*p < 0.005 compared to untreated control

(HgCl<sub>2</sub>, MeHgCl) or vehicle control MeOH (EtHgCl).

## 3. Results

### 3.1. Organic Hg species are more cytotoxic than inorganic Hg

For first insides on BeWo b30 response to all three Hg species and to find sub-toxic doses that do not affect barrier integrity, Hg cytotoxicity was assessed. Hoechst staining revealed a significant reduction of the cell number down to 90 %  $\pm$  8 % of control after treatment with 50  $\mu\text{M}$  HgCl<sub>2</sub> and almost complete loss (~10 %) at 400  $\mu\text{M}$  HgCl<sub>2</sub>. In comparison the organic Hg species MeHgCl and EtHgCl reduced the cell numbers at much lower concentrations. While MeHgCl induced significant cytotoxicity at 5  $\mu\text{M}$  with a cell number of 74 %  $\pm$  8 % of control, EtHgCl was able to reduce the cell number significantly starting from 2  $\mu\text{M}$  (89 %  $\pm$  6 % of control) (Fig. 1). As such cytotoxicity leads to the disruption of the cell barrier per se, we consequently used sub-toxic doses for this study.

### 3.2. Species-specific Hg transfer and intracellular Hg concentrations in BeWo b30 cells

For the species-specific Hg transfer the BeWo b30 transwell system was utilized allowing the investigation of cellular transport processes modelling the maternal (apical), and fetal (basolateral) compartment of the placental barrier. TEER values were not affected by the incubated Hg concentration indicating an intact barrier function (Fig. S2).

Applying different concentrations of inorganic HgCl<sub>2</sub> on the apical side of the BeWo b30 cell layer revealed a time- and concentration-dependent transfer of Hg across the trophoblast layer. 50  $\mu\text{M}$  HgCl<sub>2</sub> increased the Hg concentrations in the basolateral compartment after 24 h compared to 6 h treatment (Fig. 2A) and compared to lower HgCl<sub>2</sub> concentrations (Fig. 2B). In contrast, the organic Hg species MeHgCl, and EtHgCl both showed similar transfer behavior, when incubated on the apical side of the BeWo b30 cells for 6 as well as 24 h (Fig. 2A and B). After 24 h, both MeHgCl and EtHgCl almost reached an equilibrium (~50 % transfer) between apical and basolateral side. In comparison to the inorganic Hg species, the percentage transfer of EtHg was significantly higher even if only 1.5  $\mu\text{M}$  was applied (Fig. 2A). This indicated that the difference between the concentrations of the transferred Hg species across the placental barrier is much higher than shown for the percentage difference. Besides determining Hg transfer amounts, cellular Hg bioavailability was assessed. BeWo b30 cells showed a time-, and concentration-dependent increase in Hg concentrations normalized to protein content regardless of the incubated species. Comparing Hg contents in BeWo b30 cells upon exposure to either inorganic HgCl<sub>2</sub> or organic Hg species levels were comparable. However, as the employed concentrations for organic MeHgCl and EtHgCl were 10-fold lower

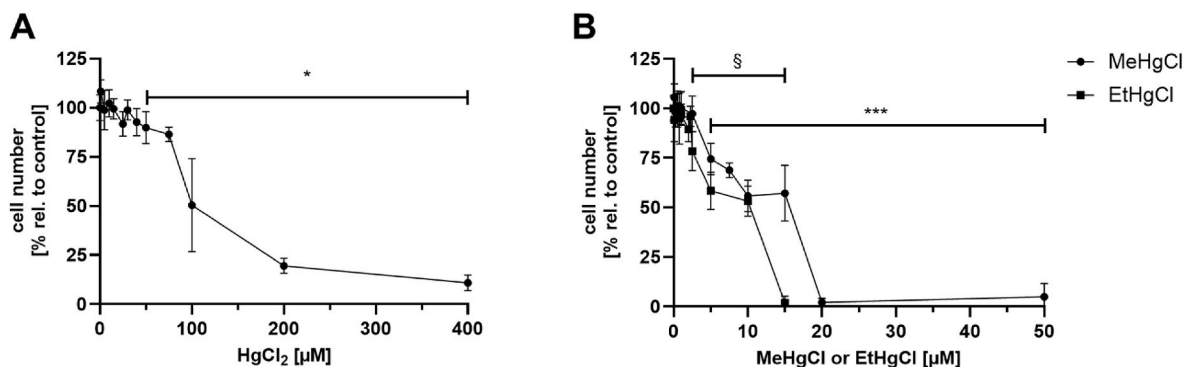
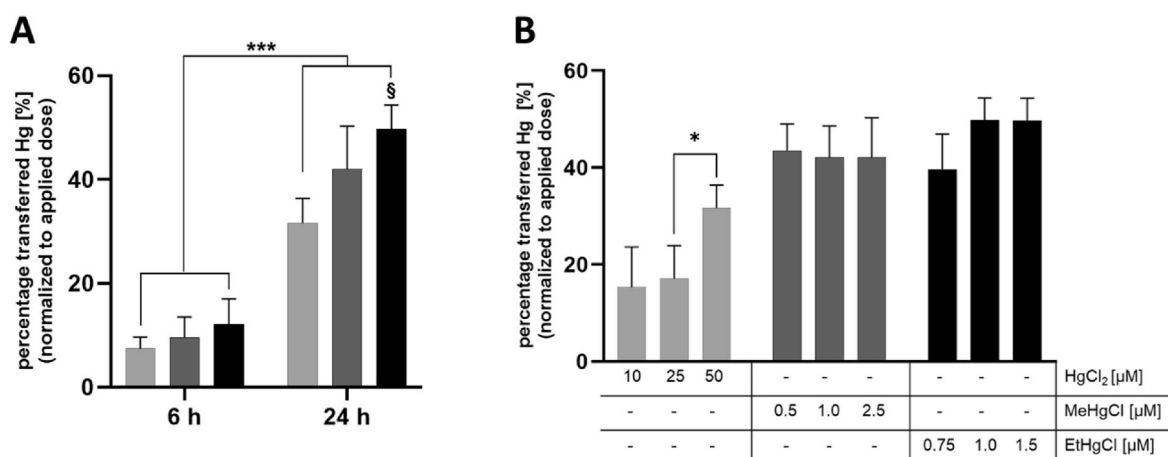


Fig. 1. (A) HgCl<sub>2</sub>, and (B) MeHgCl or EtHgCl cytotoxicity in confluent BeWo b30 cells after 24 h determined using Hoechst Assay. Shown is the mean  $\pm$  SD of at least two independent experiments with 6 technical replicates each. Significance was determined by Ordinary One-Way ANOVA with Dunnett's multiple comparison compared to untreated control, depicted as \*/§p < 0.05 (\* = HgCl<sub>2</sub>, § = EtHgCl), \*\*\*p < 0.005 (\* = MeHgCl),  $\alpha$  = 0.05 compared to untreated control.



**Fig. 2.** (A) Time-dependent transfer of  $50 \mu\text{M}$   $\text{HgCl}_2$ ,  $2.5 \mu\text{M}$   $\text{MeHgCl}$ , and  $1.5 \mu\text{M}$   $\text{EtHgCl}$ . (B) concentration-dependent transfer of inorganic  $\text{HgCl}_2$ ,  $\text{MeHgCl}$ , and  $\text{EtHgCl}$  across the confluent BeWo b30 cell layer, after 24 h of exposure. Shown is the mean + SD of at least three independent experiments (with two replicates each (6 h)). Statistical analysis is based on a One-Way ANOVA with Tukey's multiple comparison test with  $*p < 0.05$ ,  $***p < 0.001$  compared to other concentrations or time points,  $^{\text{§}}p < 0.05$  compared to other Hg species. Data for untreated controls were below the LOQ of the analytical method.

compared to  $\text{HgCl}_2$ , organic Hg bioavailability was much higher compared to inorganic (Fig. 3A and B).

To reveal potential accumulation sides of Hg at the placental barrier, each species was incubated simultaneously on the apical and basolateral side of the microporous insert. Determination of the respective Hg amount showed basolateral accumulation of Hg after incubation with  $\text{EtHgCl}$  for 24 h, which was not the case for inorganic  $\text{HgCl}_2$  and  $\text{MeHgCl}$  (Fig. 4A, B, C).

### 3.3. Barrier leakage and disruption upon inorganic and organic Hg exposure

To investigate both potential leakage and disruption of the BeWo b30 barrier the tight junction proteins  $\gamma$ -catenin and zonula occludens 1 (ZO-1) were stained using immunocytochemistry. Even if TEER values were not affected by Hg treatment (Fig. S2), staining with the antibody against  $\gamma$ -catenin and ZO-1 revealed first manifestations of barrier deformation, splits and complete rupture of single tight junctions, which could be found upon incubation at elevated dosages of each Hg species (Fig. 5). Hereby  $50 \mu\text{M}$   $\text{HgCl}_2$  led to an increased thinning of tight junctions up to complete disruption and deformations of the ZO-1

expressed tight junctions (Fig. 5B–F). An example for enhanced leakage is depicted in Fig. 5C with the formation of holes within the tight junctions upon treatment with  $2.5 \mu\text{M}$   $\text{MeHgCl}$ . In further agreement, the exposure to  $1.5 \mu\text{M}$   $\text{EtHgCl}$  led to enhanced thinning, deformation and rupture on the tight junctions (Fig. 5D–H). However, TEER values which represent the barrier tightness were not affected by these concentrations (Fig. S2). Therefore, the barrier has not been completely disrupted, yet.

### 3.4. Species-specific effects on energy-related nucleotide levels in BeWo b30 cells upon Hg exposure

Maintaining the energy metabolism in placental trophoblasts is needed to ensure their function and development. Therefore, we investigated the influence of Hg exposure on levels of adenosine- and nicotinamide-related nucleotides via LC-DAD. While incubation of BeWo b30 cells with different concentrations of  $\text{HgCl}_2$  led to significant decreased AMP levels, treatment with  $2.5 \mu\text{M}$   $\text{MeHgCl}$  significantly increased AMP levels (Fig. 6A). Although treatment with  $\text{HgCl}_2$  did not alter the levels of other energy-related nucleotides (ADP, ATP, NADH,  $\text{NAD}^+$ , NADPH; Fig. 6B, C, S1),  $2.5 \mu\text{M}$   $\text{MeHgCl}$  significantly decreased

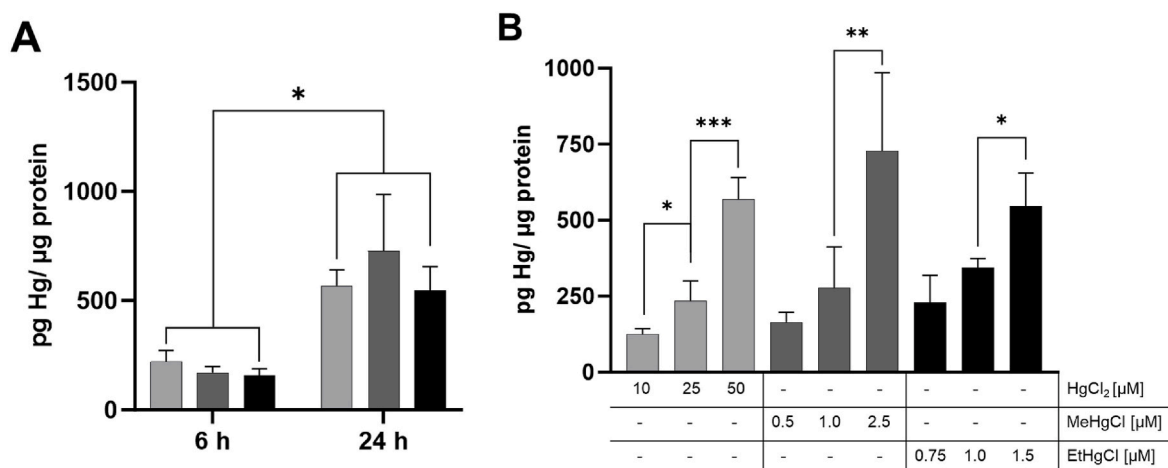


**Fig. 3.** (A) Time-dependent bioavailability of  $50 \mu\text{M}$   $\text{HgCl}_2$ ,  $2.5 \mu\text{M}$   $\text{MeHgCl}$ , and  $1.5 \mu\text{M}$   $\text{EtHgCl}$ . (B) concentration-dependent bioavailability of inorganic  $\text{HgCl}_2$ ,  $\text{MeHgCl}$ , and  $\text{EtHgCl}$  across the confluent BeWo b30 cell layer, after 24 h of exposure. Shown is the mean + SD of at least three independent experiments (with two replicates each (6 h)). Statistical analysis is based on an unpaired student's t-test with  $*p < 0.05$ ,  $**p < 0.01$ ,  $***p < 0.001$  compared to other concentrations or time points. Data for untreated controls were below the LOQ of the analytical method.

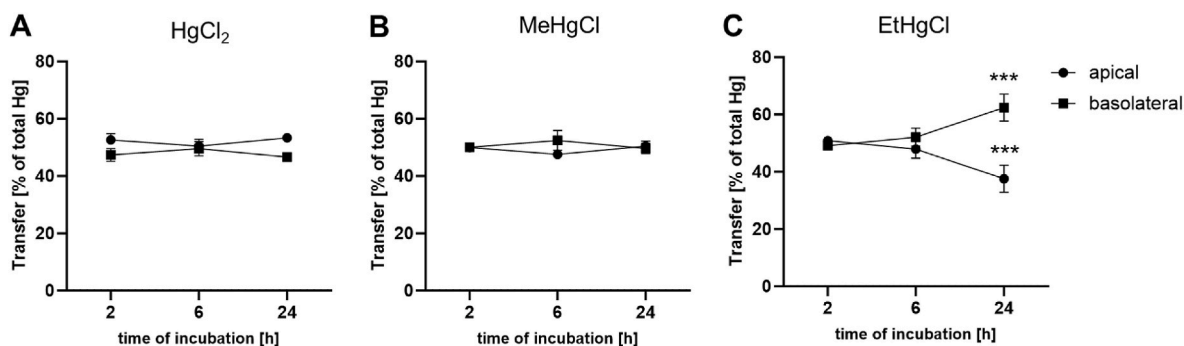


**Fig. 4.** Side-directed transfer of (A) 25  $\mu\text{M}$  inorganic  $\text{HgCl}_2$ , (B) 1.0  $\mu\text{M}$   $\text{MeHgCl}$ , and (C) 0.75  $\mu\text{M}$   $\text{EtHgCl}$  across the confluent BeWo b30 cell layer after 2, 6, and 24 h of incubation. Shown is the mean  $\pm$  SD of at least two independent experiments with two technical replicates each. Statistical analysis is based on an Ordinary One-Way ANOVA with \*\*\* $p < 0.005$  compared to 2 h time point.

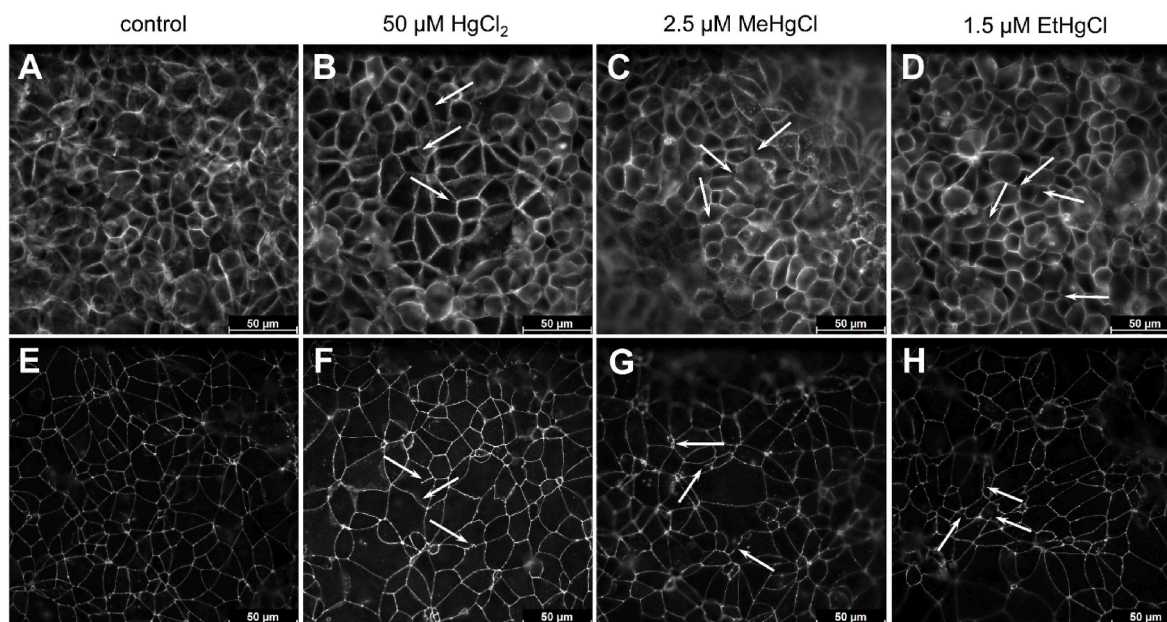


**Fig. 5.** Immunocytochemical staining of the tight junction proteins  $\gamma$ -catenin (A–D), and ZO-1 (E–H) in confluent BeWo b30 cells incubated with inorganic  $\text{HgCl}_2$  (B, F),  $\text{MeHgCl}$  (C, G), and  $\text{EtHgCl}$  (D, H) for 24 h. Arrows show leaky and disturbed tight junction sides.

ATP and NADH levels. (Fig. 6B and C). Thus, the ratio of  $\text{NAD}^+$  to NADH increased (Fig. 6D). Compared to  $\text{MeHgCl}$  exposure,  $\text{EtHgCl}$  treatment only led to significantly decreased ATP levels (Fig. 6B). Similar to  $\text{HgCl}_2$ ,  $\text{MeHgCl}$  and  $\text{EtHgCl}$  were not able to affect ADP,  $\text{NAD}^+$ , and NADPH levels (Fig. S1). The determination of the energy charge value (AEC), which is an indicator of the energy status of the cell (Atkinson and Walton, 1967) revealed a significantly increased energy status after exposure of BeWo b30 to 50  $\mu\text{M}$   $\text{HgCl}_2$ , while the organic Hg species led to a significant reduction of the energy status (2.5  $\mu\text{M}$   $\text{MeHgCl}$ , 0.75  $\mu\text{M}$ , and 1.5  $\mu\text{M}$   $\text{EtHgCl}$ , respectively) (Fig. 6E).

### 3.5. Hg inhibits total SOD and GPX activity in BeWo b30 cells

Changes in the energy related nucleotide levels may hint at mitochondrial dysfunction which may be the cause or consequence of oxidative stress conditions. Therefore, the activity of the antioxidative defense associated enzyme families superoxide dismutase (SOD) and glutathione peroxidase (GPX) was determined. Data revealed significantly inhibited SOD activity by  $\text{HgCl}_2$  after exposure with the highest dose, while  $\text{MeHgCl}$  led to significantly decreased SOD activity after incubation with the lowest dose. Comparing all incubated  $\text{MeHgCl}$  doses revealed a trend towards an increase of SOD activity (Fig. 7A). On the

contrary all three Hg species significantly inhibited total GPX activity to at least 50 % (Fig. 7B).

### 3.6. Perturbed glutathione metabolism due to Hg exposure

Since Hg possesses a high affinity to thiol-containing enzymes and proteins, glutathione is a vulnerable target affecting the antioxidative defense metabolism in placental trophoblasts. Therefore, GSH and GSSG levels were determined in BeWo b30 cells 24 h after Hg exposure via a recently published LC-MS/MS method (Thiel et al., 2023). Comparing inorganic  $\text{HgCl}_2$  exposure to organic Hg species GSH and GSSG levels were altered in different ways.  $\text{HgCl}_2$  treatment led to significantly increased GSH and GSSG levels in a concentration-dependent manner for the latter (Fig. 8A and B). Conversely, GSH levels were significantly decreased after exposure to 1.5  $\mu\text{M}$   $\text{EtHgCl}$ , but not for  $\text{MeHgCl}$  (Fig. 8A). Although  $\text{MeHgCl}$  did not alter single GSH and GSSG levels, the ratio between these two recycling forms of glutathione was significantly decreased upon exposure to 2.5  $\mu\text{M}$   $\text{MeHgCl}$ , to 25  $\mu\text{M}$  and 50  $\mu\text{M}$   $\text{HgCl}_2$ , and to 1.0  $\mu\text{M}$  and 1.5  $\mu\text{M}$   $\text{EtHgCl}$  as well (Fig. 8C).

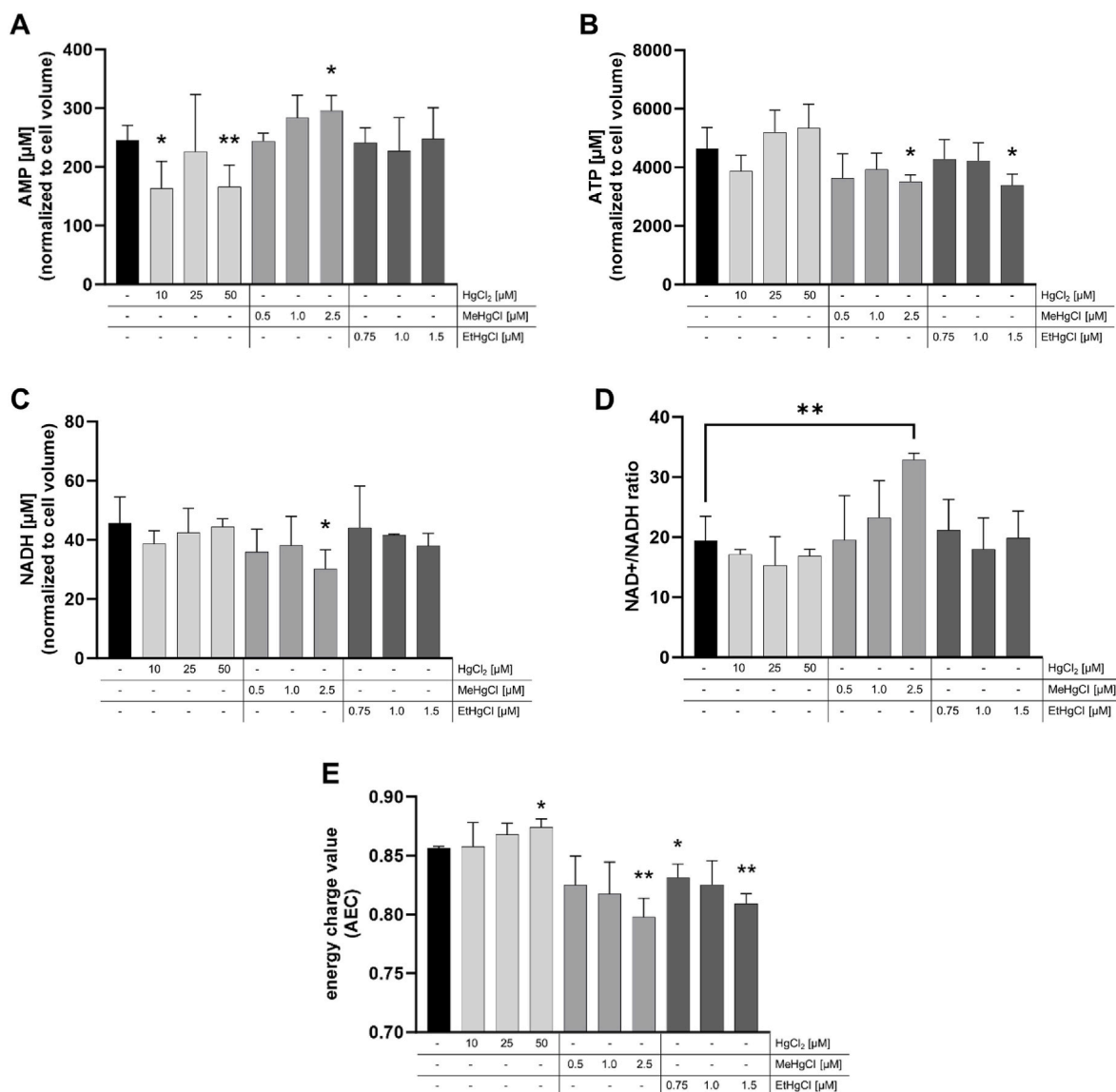


Fig. 6. Levels of energy-related nucleotides determined via LC-DAD in confluent BeWo b30 cells incubated with inorganic HgCl<sub>2</sub>, MeHgCl, and EtHgCl for 24 h. Shown is the mean + SD of (A) AMP levels, (B) ATP levels, (C) NADH levels, (D) NAD<sup>+</sup>/NADH ratio, and (E) energy charge value of at least three independent experiments. Statistical analysis is based on an unpaired student's t-test with \*p < 0.05, \*\*p < 0.01 compared to untreated control.

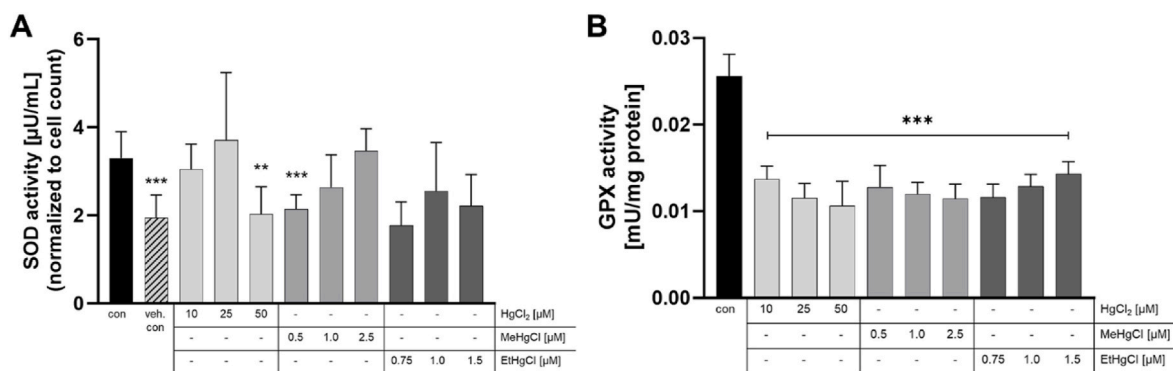
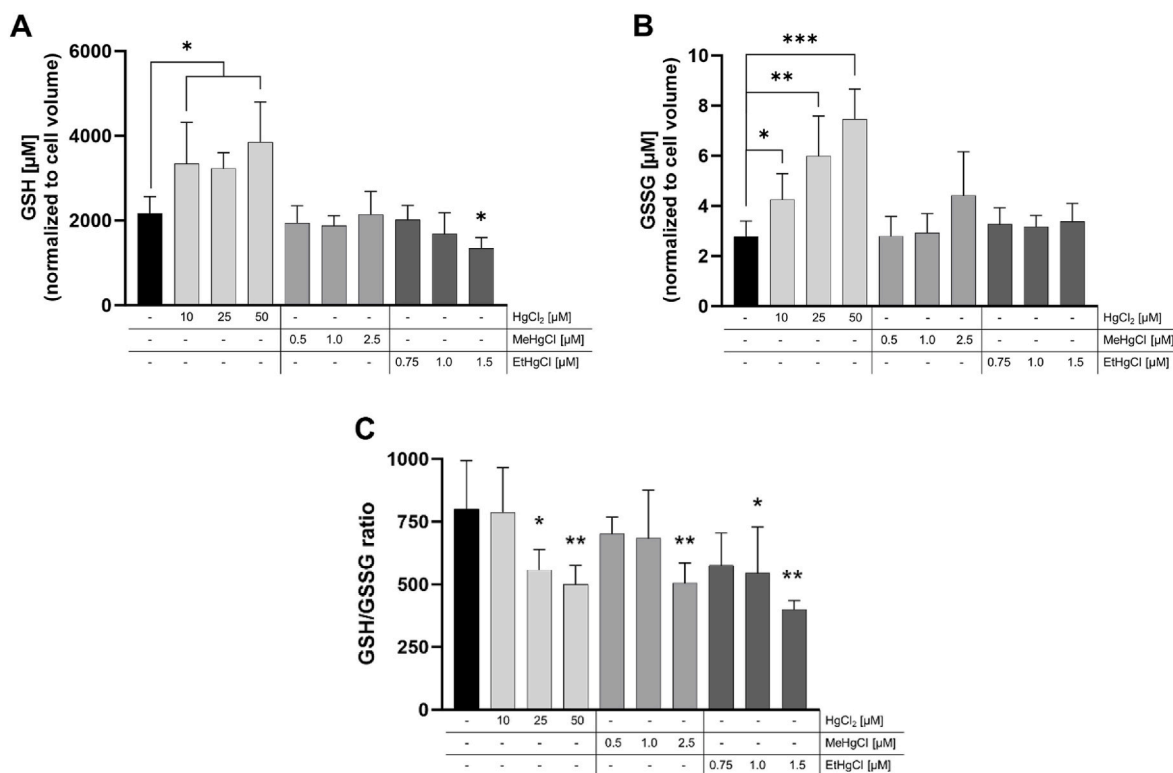


Fig. 7. SOD activity [ $\mu$ U/mL] and GPX activity [mU/mg protein] in confluent BeWo b30 cells incubated with inorganic HgCl<sub>2</sub>, MeHgCl, and EtHgCl for 24 h. Shown is the mean + SD of (A) SOD activity, and (B) GPX activity, of at least three independent experiments. Statistical analysis is based on an unpaired student's t-test with \*\*p < 0.01, \*\*\*p < 0.001 compared to respective control (HgCl<sub>2</sub> and MeHgCl vs. control; EtHgCl vs. vehicle control).



**Fig. 8.** (A) GSH levels, (B) GSSG levels, and (C) GSH/GSSG ratio determined via LC-MS/MS in confluent BeWo b30 cells incubated with inorganic HgCl<sub>2</sub>, MeHgCl, and EtHgCl for 24 h. Shown is the mean + SD of at least three independent experiments. Statistical analysis is based on an unpaired student's t-test with \*p < 0.05, \*\*p < 0.01, \*\*\*p < 0.001 compared to untreated control.

### 3.7. Hg species-specific induction of combined cell death mechanisms

Investigating the induction of apoptosis or necrosis upon 24 h treatment with the three different Hg species revealed the induction of both cell death mechanisms. While caspase-3 activity, as a marker for apoptosis, was significantly enhanced by 25 μM and 50 μM HgCl<sub>2</sub> as well as all tested concentrations for EtHgCl up to 8-fold, AFC cleavage was firstly decreased at low MeHgCl concentrations but raised up to 3-fold when incubating the highest MeHgCl concentration of 2.5 μM (Fig. 9A). LDH, a marker for necrosis, was released after 24 h treatment in BeWo b30 cells at all tested concentrations of all Hg species. The most pronounced effects were obtained by treatment with HgCl<sub>2</sub>. In comparison to that the organic Hg species showed a lower but significant increase in LDH release which was concentration-dependent for MeHgCl but not for EtHgCl (Fig. 9B).

### 4. Discussion

Recent studies have highlighted that increased MeHg levels in fish are of special concern for vulnerable sub-populations like pregnant women (Fechner et al., 2022). Therefore, this study is to our knowledge the first analyzing Hg species-specific transfer and toxicity mechanisms in a placental trophoblast cell line in a comparative manner taking environmental (HgCl<sub>2</sub>), nutritive (MeHgCl) and medical exposure (EtHgCl) into account. Doses used in this study are 5- to 10-fold higher as physiologically reachable in blood after high fish consumption but rather include a low-level, long term exposure (24 h of incubation) and accumulation in placental tissues reaching placental concentrations from 4 to 52 ng/g placental wet weight (Akiyama et al., 2022; Freire et al., 2019; Iwai-Shimada et al., 2019; Lohren et al., 2016). Additionally, applying higher Hg doses is needed to identify potential target sides of Hg-induced toxicity in placental barrier building cells to gain more

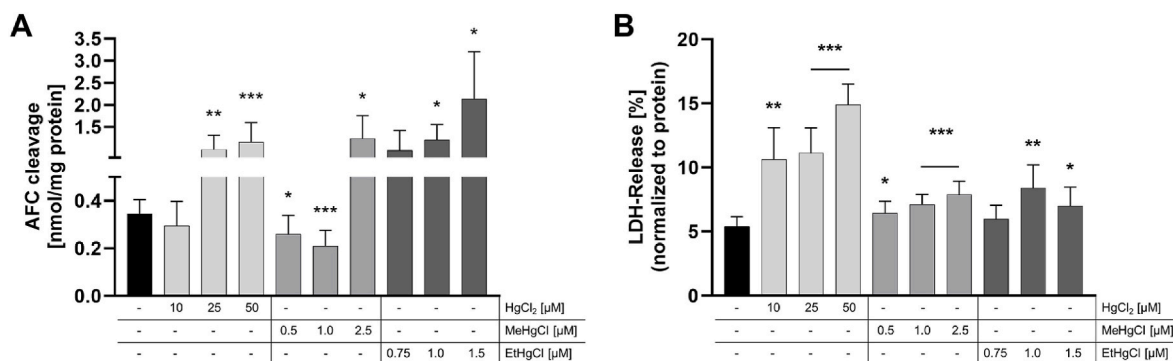


**Fig. 9.** (A) Caspase-3 activity (AFC cleavage) [nmol/mg protein] and (B) lactate dehydrogenase release [%] normalized to protein in confluent BeWo b30 cells incubated with inorganic HgCl<sub>2</sub>, MeHgCl, and EtHgCl for 24 h. Shown is the mean + SD of at least three independent experiments. Statistical analysis is based on an unpaired student's t-test with \*p < 0.05, \*\*p < 0.01, \*\*\*p < 0.001 compared to untreated control.

insights into the underlying mechanism. However, the transferability to human exposure is therefore limited.

Importantly, we find that Hg is transferred time- and species-dependently across the BeWo b30 *in vitro* model, resembling placental trophoblasts. Both organic Hg species were transferred to a much higher extent compared to inorganic Hg, almost reaching an equilibrium between the apical (maternal) and the basolateral (fetal) side after 24 h of treatment (Fig. 2A and B). Interestingly, treatment with 50  $\mu\text{M}$   $\text{HgCl}_2$  led to a significantly higher transfer rate compared to the other tested  $\text{HgCl}_2$  dosages (Fig. 2B). A study by Lohren et al. (2016) investigating Hg-species specific transfer across primary porcine brain capillary endothelial cells (PBCECs) modelling the blood-brain barrier *in vitro* showed comparable results regarding species specificity (Lohren et al., 2016). In the blood-brain barrier model the two organo-Hg species showed higher transfer rates ( $\sim 75\%$  1  $\mu\text{M}$  MeHgCl,  $\sim 70\%$  1  $\mu\text{M}$  thiomersal, with EtHg as metabolite) compared to inorganic  $\text{HgCl}_2$ , for which transfer rates to the basolateral compartment were lower than 10%. In our study, basolateral transfer rates of  $\text{HgCl}_2$  were higher than 10% (Fig. 2B), however, higher  $\text{HgCl}_2$  concentrations were used for our placental barrier model. Ganapathy et al. have investigated the transfer of MeHg in the form of radiolabeled MeHg-cysteine in BeWo cells. They saw a time-dependent MeHg-cysteine uptake in a time course of 60 min of incubation with 5  $\mu\text{M}$  MeHg-cysteine. A time-dependent Hg transfer could be verified in BeWo b30 cells comparing basolateral transfer rates after 6 and 24 h of incubation (Fig. 2A) (Ganapathy et al., 2021). Absent concentration-dependency may be explained by a constant transfer across the barrier either due to diffusion processes or unhindered active transport. One thereto proposed mechanism is that Hg bound to the amino acid cysteine mimics the structure of L-methionine and therefore being transported *via* amino acid transporters of the L-type like LAT1 or LAT2, which are also expressed in placental trophoblasts. This is mainly the case for the organic Hg species which were also more readily transferred across the placental barrier due to their higher lipophilicity. Therefore, lower  $\text{HgCl}_2$  transfer across the BeWo b30 cell layer compared to organic Hg in this study may be attributed to a lower lipophilicity but is not completely absent like other studies reported (Ask et al., 2002; Balthasar et al., 2017; Oliveira et al., 2015). Next to Hg transfer we determined Hg-species bioavailability in BeWo b30 cells, which was time- and concentration-dependently increased. Comparing Hg amounts, all three species showed similar results comparing the lowest to highest dose, however incubated concentrations differ immensely (Fig. 3A and B). Lohren et al. who also compared all three Hg species saw higher Hg bioavailability in the PBCECs but had an incubation duration of 72 h. However, MeHg seems to be more bioavailable in the brain capillary cells compared to EtHg while in placenta cells no significant changes between MeHg and EtHg were detectable (Lohren et al., 2016). Incubation on either apical and basolateral side of the BeWo b30 cell layer revealed basolateral Hg enrichment upon 24 h EtHgCl exposure (Fig. 4C). This may be attributed to diffusion processes at the cell layer due to the lipophilicity of EtHgCl compared to  $\text{HgCl}_2$  as proposed from Lohren et al. in an *in vitro* model of the blood-brain barrier (Lohren et al., 2016). However, it has still to be clarified why MeHgCl is behaving differently compared to EtHgCl.

Higher transfer rates of the highest dose of  $\text{HgCl}_2$  compared to the lower doses hinted towards an increased permeability at the barrier. This higher permeability may be attributed to beginning cytotoxic modes of action. 50  $\mu\text{M}$   $\text{HgCl}_2$  showed already significant effects in the cytotoxicity assessment using Hoechst assay (Fig. 1A). Additionally, the staining of the tight junction proteins  $\gamma$ -catenin and ZO-1 verified this hypothesis. All three species in their highest dose (50  $\mu\text{M}$   $\text{HgCl}_2$ , 2.5  $\mu\text{M}$  MeHgCl, and 1.5  $\mu\text{M}$  EtHgCl) were able to perturb the barrier integrity by leading to splints, deformations up to complete rupture in the two tight junction proteins ZO-1 and  $\gamma$ -catenin in BeWo b30 cells after 24 h of incubation (Fig. 5). Alterations in ZO-1 were described beforehand in several studies applying an intestinal barrier and mouse model. Here, deformations were observed as well as a significant reduction in the

gene expression of ZO-1 after 24 h treatment with 1 mg/L  $\text{Hg}(\text{NO}_3)_2$  or MeHgCl in the barrier model (corresponding to 5  $\mu\text{M}$ ) and 5–10 mg Hg/L for 4 months in a mouse model (Rodríguez-Viso et al., 2022, 2023; Vázquez et al., 2014).

In placental trophoblasts, potential underlying mechanisms of toxicity are scarcely investigated. Therefore, next to transfer we were also interested in potential target mechanisms regarding Hg species-specific toxicity. Here, target sides of Hg-induced toxicity include the energy-, and antioxidative defense system with decreased ATP levels, and binding to thiol-containing enzymes and proteins which are mandatory in the prevention of oxidative stress. Data on energy-related nucleotides revealed decreased AMP levels for inorganic Hg, while the organic species significantly decreased ATP levels (Fig. 6A and B). Further, MeHg increased AMP and decreased NADH levels, which resulted in an increased  $\text{NAD}^+/\text{NADH}$  ratio (Fig. 6A–C, D). However, to date it is not completely understood, why NADH was reduced. Studies by Hamdy et al. have revealed that NADH can interact with Hg by reduction to a  $\text{NAD-Hg}^+$  complex (Hamdy and Noyes, 1977). This might lead to limited availability of NADH as a co-factor for various important processes in cellular defense mechanisms or respiration by complex I in the mitochondrial electron transport chain. To get an overview of the overall energy metabolism in cells described by a shift in the equilibrium between ADP and ATP, the energy charge value was determined. Even if alterations due to inorganic Hg, MeHg and EtHg exposure in the single nucleotide levels were not substantial, it was clearly shown that organic Hg species are reducing the energy charge value, while inorganic Hg increased it (Fig. 6E). Therefore, mechanisms influencing energy metabolism seem to differ. In conditions of cellular energy stress due to perturbed energy homeostasis and decreasing ATP levels the AMP-activated protein kinase (AMPK) is activated preventing the utilization of ATP and promoting catabolic processes generating ATP (Garcia and Shaw, 2017). Studies in neuronal PC12 cells have shown increased protein expression of phosphorylated (activated) AMPK after 24 h treatment with MeHg concentrations from 1.25 to 5  $\mu\text{M}$ , which may lead to changes of mitochondrial dynamics. AMPK additionally activates processes of mitochondrial fission which further activate mitophagy- and autophagy-associated mechanisms. Therefore, reduction in the energy charge observed in BeWo b30 cells may be a first hint towards mitochondrial-associated toxicity of MeHg but also EtHg which shows similar effects (Hu et al., 2024). Regarding the energy charge value, inorganic Hg shows the complete opposite. Even if it is proposed that Hg interferes with protein thiols of important enzymes within cells leading to inhibition, Nesci et al. found out, that  $\text{HgCl}_2$  stimulates the mitochondrial  $\text{F}_1\text{F}_0$ -ATPase in swine heart mitochondria. Nesci et al. assume that the activation of the ATPase maintains the polarization of the inner mitochondrial membranes and ionic homeostasis in case of the inhibition of respiration, which may explain higher ATP levels compared to the organic species (Nesci et al., 2016). On the other side the activation of the ATPase may also lead to the reduction of ATP, since ATP is consumed in order to maintain the membrane potential (Zharova et al., 2023). Therefore, the exact mechanisms on the steady state in ATP upon  $\text{HgCl}_2$  treatment has still to be elucidated. The reduction in AMP levels however may be attributed to  $\text{HgCl}_2$  inhibiting the ATP diphosphatase, which was shown by Oliveria et al. in the cerebral cortex of developing rats (Oliveira et al., 1994). Therefore, Hg interference in the cellular energy metabolism of BeWo b30 cells seem to include perturbations of the adenosine nucleotide equilibrium which may be the cause or consequence of mitochondrial dysfunction or inhibition of important processes in ATP, ADP and AMP generation by binding to thiol-rich enzyme sites.

Changes in the energy metabolism of cells has often been linked to oxidative stress conditions, which has been discussed in the context of Hg-induced toxicity (Farina et al., 2011). We thus determined the activity of total SOD and GPX both involved in the antioxidative defense. In BeWo b30 cells SOD activity was decreased upon incubation with the highest dose of  $\text{HgCl}_2$ , while MeHg decreased SOD activity only in the

lowest dose and a trend towards an increase compared to untreated control conditions with increasing MeHg concentrations was observed (Fig. 7A). Studies in primary trophoblasts have revealed that decreased SOD activity correlated with the increased formation of superoxide radicals (Wang and Walsh, 2001). Additionally, SODs possess a cysteine-rich center which is a prominent target for Hg binding, therefore unavailable for the detoxification for superoxide radicals (Kumar et al., 2020; Shimojo et al., 2002). In line with this, the decrease in GPX activity is supposed to be due to inhibition by Hg binding to selenocysteine in the active center of GPX (Fig. 7B) (Branco et al., 2012). Therefore, superoxide radicals cannot be scavenged properly and those which are reduced to H<sub>2</sub>O<sub>2</sub> cannot be detoxified further due to limited GPX activity. Hg species-specific effects can also be observed in the redox cycling of GSH/GSSG in BeWo b30 cells. Inorganic Hg dose-dependently increased GSSG levels with a direct response in increased GSH levels, while EtHg led to a reduction in GSH (Fig. 8A and B). For MeHg changes in the levels of GSH and GSSG were not observable, however regarding the GSH/GSSG ratio incubating 2.5 μM MeHg for 24 h resulted in a significant reduction of 35 % compared to untreated control. This was also the case for inorganic Hg and EtHg (Fig. 8C). Due to the sulfur group from the cysteine residue of GSH, binding of Hg is the most discussed mechanism regarding changes of GSH/GSSG levels. This is presumably the reason for decreased GSH levels after 24 h EtHg exposure in BeWo b30 cells. Inorganic Hg exposure seems to follow a more oxidative stress pattern. GSSG was increasing dose-dependently upon HgCl<sub>2</sub> challenge, accompanied by the cellular response of increased GSH to be available for further detoxification (Fig. 8A and B). Potentially involved in the formation of GSH is the γ-glutamyl transpeptidase which has been shown to correlate with increasing Hg levels and was discussed as a marker of Hg exposure (Dierickx, 1980; Tinkov et al., 2014). The γ-glutamyl transpeptidase, which can also be found in the placenta, is located at the cell membrane cleaving extracellular GSH to provide cysteine for intracellular GSH synthesis mainly in case of cells exposed to compounds which are able to deplete GSH to prepare them for increased oxidative stress (Dubnov-Raz et al., 2006; Hanigan, 2014). To date it is not clear, why inorganic Hg is behaving differently than the organic species which are depleting GSH levels.

Due to the fact, that important processes in the antioxidative defense system and energy metabolism are perturbed by Hg species, cell death seems likely. For this we employed the cleavage of the caspase-3 and 7 substrate DEVD-AFC and LDH release for apoptosis and necrosis detection, respectively. Data suggested a significant activation of the caspases upon incubation with inorganic Hg and EtHg, while MeHg showed a reduced AFC cleavage in the low doses followed by an increase at the highest dose of 2.5 μM (Fig. 9A). For LDH release, incubation with all Hg species resulted in significantly higher LDH release compared to control, and the effect for inorganic Hg was the most distinct (Fig. 9B). Induction of apoptosis upon treatment with HgCl<sub>2</sub> was observed in the trophoblastic cell line JEG-3 validating our results in BeWo b30 cells (Kim et al., 2021; Palomar et al., 2023). EtHg seems to follow similar mechanism to inorganic Hg, which can be explained by EtHg more readily decomposing to inorganic Hg compared to MeHg. This may be additionally the case while EtHg is more cytotoxic than MeHg because in case EtHg is decomposed within the cell, inorganic Hg cannot pass the cell membrane due to its limited lipophilicity (de Souza Prestes et al., 2023). A study in peripheral blood mononuclear cells (PBMCs) has shown an increased apoptotic population after 24 h of incubation with EtHg which was not the case for MeHg (de Souza Prestes et al., 2023). However, in HTR-8/SVneo cells, which resemble placental trophoblasts, MeHg was able to induce apoptosis. This was observed in BeWo b30 cells at the highest concentration of 2.5 μM MeHg (Liao et al., 2021). Interestingly, MeHg further decreased caspase activity at lower concentrations which was described for different breast cancer cell lines. One explanation may be Hg binding to the cysteine in the active site of caspase-3 which is normally cleaving the aspartic acid from the target

protein leading to inhibition (Asadi et al., 2022; McCabe et al., 2005; Wallace, 2015). Increased LDH release which was observed for all Hg species in BeWo b30 trophoblasts (Fig. 9B) was similarly seen by a study from Lohren et al. who investigated all three Hg species in human astrocyte and neuron culture. There, all three species were able to induce LDH release however not as pronounced as in placental BeWo b30 cells (Lohren et al., 2015). Since all three species are able to induce either caspase activity as well as LDH release the mechanism of cell death in BeWo b30 cells seem to follow a mixed type. Studies in murine macrophages have shown an increase in TNFα accompanied by increased markers of necrosis and apoptosis which may indicate necroptosis as an uncontrolled inflammatory cell death cascade as a potential underlying cell death mechanism (Kim and Sharma, 2004; Ye et al., 2023). Taken together these findings regarding perturbed barrier integrity, energy metabolism and induction of cell death mechanisms, the risk for higher Hg exposure *in utero* but also to other xenobiotics available in maternal blood increases. In the most adverse setting this may put fetal and placental development in jeopardy raising concerns for further pregnancy complications including miscarriage (Bjørklund et al., 2019). Nevertheless, this study revealed potential targets of Hg-induced toxicity in a placental trophoblast model, Hg species concentrations applied are beyond physiological reachable concentrations. Therefore, transferability of gained results on the exposure scenario *in vivo* is limited. In future studies target mechanisms will be verified for physiological Hg concentrations at the placental barrier also using primary trophoblast culture to reveal metabolic dysfunction of trophoblasts cells potentially affecting the development of the fetus. Regarding Hg bioavailability, the determination of total Hg amounts gives first insights into Hg species-specific cellular Hg amounts and transfer behavior in placental trophoblasts, however, Hg speciation analysis realized in future studies will further clarify if organic Hg species are transformed during transfer and if species-specific effects are dependent on Hg amount in general or on the species itself.

## 5. Conclusion and outlook

Although it has been known before that MeHg is able to cross the placental barrier leading to adverse effects on the developing fetal brain, information on the exact transfer and toxicity mechanisms of different Hg species present in the environment, food and used in medical applications is scarce. Since Hg species like inorganic Hg and the two organic Hg species MeHg and EtHg have been shown to follow different toxicological profiles, their effects on trophoblast cells have not been elucidated in detail, yet. Data obtained in placental trophoblasts revealed species-specific effects in the transfer of Hg across the trophoblast layer with the organic species being the most bioavailable. Increased transfer could be correlated with changes in the integrity of the tight junction proteins ZO-1 and γ-catenin indicating higher permeability after applying the highest dosage. Hg-induced toxicity assessed by using endpoints to investigate antioxidative defense, and energy metabolism revealed changes in the equilibrium between the energy nucleotides AMP, ADP and ATP, decreased activity of SOD for HgCl<sub>2</sub> and MeHg and decreased activity of GPX for all three species. The redox cycling of GSH was also perturbed species-specifically. This data is a first hint for potential mitochondria-associated toxicity but also include the possibility of the induction of reactive oxygen species and necroptosis, which is a combination of inflammatory and cascade-dependent form of cell death which has to be elucidated in future studies. However, revealing important targets of Hg-induced toxicity and the understanding of Hg-dependent transfer processes in placenta barrier building cells enhances the data availability for the risk characterization during pregnancy and may pave the way for potential therapeutic strategies preventing Hg-induced adverse effects for the developing fetus.

## CRedit authorship contribution statement

**Vivien Michaelis:** Writing – original draft, Visualization, Validation, Methodology, Investigation, Formal analysis, Data curation, Conceptualization. **Laura Klemens:** Writing – review & editing, Visualization, Methodology, Formal analysis. **Alicia Thiel:** Writing – review & editing, Methodology. **Anna Gremme:** Writing – review & editing, Methodology. **Maria Schwarz:** Writing – review & editing, Methodology. **Anna P. Kipp:** Writing – review & editing, Methodology. **Hans Zischka:** Writing – review & editing.

## Declaration of competing interest

There are no conflicts of interest to declare.

## Acknowledgements

We thank Alan L. Schwartz (Washington University School of Medicine, MO, USA) for the permission to use BeWo subclone b30 and Tina Buerki-Thurnherr (EMPA, Swiss Federal Laboratories for Materials Science and Technology, St. Gallen, Switzerland) for providing the BeWo b30 cells. We also thank Julia Bornhorst for her laboratory support and intellectual input for this study.

## Appendix A. Supplementary data

Supplementary data to this article can be found online at <https://doi.org/10.1016/j.chemosphere.2024.143870>.

## Data availability

Data will be made available on request.

## References

- Aengenheister, L., Keesend, K., Muoth, C., Schönenberger, R., Diener, L., Wick, P., Buerki-Thurnherr, T., 2018. An advanced human in vitro co-culture model for translocation studies across the placental barrier. *Sci. Rep.* 8, 5388.
- Akiyama, M., Shinkai, Y., Yamakawa, H., Kim, Y.-G., Kumagai, Y., 2022. Potentiation of methylmercury toxicity by combined metal exposure: in vitro and in vivo models of a restricted metal exposome. *Chemosphere* 299, 134374.
- Albers, A., Gies, U., Raatschen, H.J., Klintschar, M., 2020. Another umbrella murder? - a rare case of Minamata disease. *Forensic Sci. Med. Pathol.* 16, 504–509.
- Alissa, E.M., Ferns, G.A., 2011. Heavy metal poisoning and cardiovascular disease. *J. Toxicol.* 2011, 870125.
- Asadi, M., Taghizadeh, S., Kaviani, E., Vakili, O., Taheri-Anganeh, M., Tahamtan, M., Savardashtaki, A., 2022. Caspase-3: structure, function, and biotechnological aspects. *Biotechnol. Appl. Biochem.* 69, 1633–1645.
- Ask, K., Akesson, A., Berglund, M., Vahter, M., 2002. Inorganic mercury and methylmercury in placentas of Swedish women. *Environ. Health Perspect.* 110, 523–526.
- Atkinson, D.E., Walton, G.M., 1967. Adenosine triphosphate conservation in metabolic regulation: rat liver citrate cleavage enzyme. *J. Biol. Chem.* 242, 3239–3241.
- Balthasar, C., Stangl, H., Widhalm, R., Granitzer, S., Hengstschläger, M., Gundacker, C., 2017. Methylmercury uptake into BeWo cells depends on LAT2-4F2hc, a system L amino acid transporter. *Int. J. Mol. Sci.* 18.
- Björklund, G., Chirumbolo, S., Dadar, M., Pivina, L., Lindh, U., Butnariu, M., Aaseth, J., 2019. Mercury exposure and its effects on fertility and pregnancy outcome. *Basic Clin. Pharmacol. Toxicol.* 125, 317–327.
- Björklund, O., Kahlström, J., Salmi, P., Ogren, S.O., Vahter, M., Chen, J.F., Fredholm, B. B., Daré, E., 2007. The effects of methylmercury on motor activity are sex- and age-dependent, and modulated by genetic deletion of adenosine receptors and caffeine administration. *Toxicology* 241, 119–133.
- Bornhorst, J., Ebert, F., Lohren, H., Humpf, H.U., Karst, U., Schwerdtle, T., 2012. Effects of manganese and arsenic species on the level of energy related nucleotides in human cells. *Metallomics* 4, 297–306.
- Branco, V., Canário, J., Lu, J., Holmgren, A., Carvalho, C., 2012. Mercury and selenium interaction in vivo: effects on thioredoxin reductase and glutathione peroxidase. *Free Radic. Biol. Med.* 52, 781–793.
- Brocza, F.M., Rafaj, P., Sander, R., Wagner, F., Jones, J.M., 2024. Global scenarios of anthropogenic mercury emissions. *Atmos. Chem. Phys.* 24, 7385–7404.
- de Souza Prestes, A., Vargas, J.L.S., Dos Santos, M.M., Druzian, G.T., da Rocha, J.T., Aschner, M., Barbosa, N.V., 2023. EtHg is more toxic than MeHg to human peripheral blood mononuclear cells: involvement of apoptotic, mitochondrial, oxidative and proliferative parameters. *Biochim. Biophys. Acta Gen. Subj.* 1867, 130446.
- Dierickx, P.J., 1980. Urinary gamma-glutamyl transferase as a specific marker for mercury after heavy metal treatment of rats. *Toxicol. Lett.* 6, 235–238.
- Dorea, J.G., Barbosa, A.C., Silva, G.S., 2006. Fish mercury bioaccumulation as a function of feeding behavior and hydrological cycles of the Rio Negro, Amazon. *Comp. Biochem. Physiol. C Toxicol. Pharmacol.* 142, 275–283.
- Dórea, J.G., Farina, M., Rocha, J.B., 2013. Toxicity of ethylmercury (and Thimerosal): a comparison with methylmercury. *J. Appl. Toxicol.* 33, 700–711.
- Dubnov-Raz, G., Shapiro, R., Merlob, P., 2006. Maternal lamotrigine treatment and elevated neonatal gamma-glutamyl transpeptidase. *Pediatr. Neurol.* 35, 220–222.
- EFSA, 2012. Scientific Opinion on the risk for public health related to the presence of mercury and methylmercury in food. *EFSA J.* 10, 2985.
- FAO/WHO, 2007. Safety evaluation of certain food additives and contaminants. Methyl Mercury. *WHO Food Addit. Ser.* 58, 269–315.
- FAO/WHO, 2011. Safety evaluation of certain food additives and contaminants. Mercury. *WHO Food Addit. Ser.* 63, 605–685.
- Farina, M., Rocha, J.B., Aschner, M., 2011. Mechanisms of methylmercury-induced neurotoxicity: evidence from experimental studies. *Life Sci.* 89, 555–563.
- Fechner, C., Hackethal, C., Höpfner, T., Dietrich, J., Bloch, D., Lindtner, O., Sarvan, I., 2022. Results of the BfR MEAL Study: in Germany, mercury is mostly contained in fish and seafood while cadmium, lead, and nickel are present in a broad spectrum of foods. *Food Chem. X* 14, 100326.
- Freire, C., Amaya, E., Gil, F., Murcia, M., S, L.L., Casas, M., Vrijheid, M., Lertxundi, A., Irizar, A., Fernández-Tardón, G., Castro-Delgado, R.V., Olea, N., Fernández, M.F., 2019. Placental metal concentrations and birth outcomes: the Environment and Childhood (INMA) project. *Int. J. Hyg Environ. Health* 222, 468–478.
- Friedrich, H.K.J., Michalke, B., Karst, U., Michaelis, V., 2024. Using L-cysteine to enhance calibration range and prevent a memory effect in mercury analysis of complex samples via ICP-OES. *J. Trace Elem. Med. Biol.* 84, 127467.
- Ganapathy, S., Farrell, E.R., Vaghela, S., Joshee, L., Ford, E.G.t., Uchakina, O., McKallip, R.J., Barkin, J.L., Bridges, C.C., 2021. Transport and toxicity of methylmercury-cysteine in cultured BeWo cells. *Int. J. Mol. Sci.* 23.
- Gao, J., Wang, L., 2018. Ecological and human health risk assessments in the context of soil heavy metal pollution in a typical industrial area of Shanghai, China. *Environ. Sci. Pollut. Res. Int.* 25, 27090–27105.
- Garcia, D., Shaw, R.J., 2017. AMPK: mechanisms of cellular energy sensing and restoration of metabolic balance. *Mol. Cell* 66, 789–800.
- Hamdy, M.K., Noyes, O.R., 1977. Effect of mercury on NADH and the protective role of oxalacetate. *Bull. Environ. Contam. Toxicol.* 17, 112–120.
- Hanigan, M.H., 2014. Chapter three - gamma-glutamyl transpeptidase: redox regulation and drug resistance. In: Townsend, D.M., Tew, K.D. (Eds.), *Advances in Cancer Research*. Academic Press.
- Hoffmeyer, R.E., Singh, S.P., Doonan, C.J., Ross, A.R., Hughes, R.J., Pickering, I.J., George, G.N., 2006. Molecular mimicry in mercury toxicology. *Chem. Res. Toxicol.* 19, 753–759.
- Hu, Y., Tian, C., Chen, F., Zhang, A., Wang, W., 2024. The mystery of methylmercury-perturbed calcium homeostasis: AMPK-DRP1-dependent mitochondrial fission initiates ER-mitochondria contact formation. *Sci. Total Environ.* 923, 171398.
- Iwai-Shimada, M., Kameo, S., Nakai, K., Yaginuma-Sakurai, K., Tatsuta, N., Kurokawa, N., Nakayama, S.F., Satoh, H., 2019. Exposure profile of mercury, lead, cadmium, arsenic, antimony, copper, selenium and zinc in maternal blood, cord blood and placenta: the Tohoku Study of Child Development in Japan. *Environ. Health Prev. Med.* 24, 35.
- Kim, M.J., Park, J., Kim, J., Kim, J.Y., An, M.J., Shin, G.S., Lee, H.M., Kim, C.H., Kim, J. W., 2021. Transcriptome analysis reveals HgCl<sub>2</sub> induces apoptotic cell death in human lung carcinoma H1299 cells through caspase-3-independent pathway. *Int. J. Mol. Sci.* 22.
- Kim, S.H., Sharma, R.P., 2004. Mercury-induced apoptosis and necrosis in murine macrophages: role of calcium-induced reactive oxygen species and p38 mitogen-activated protein kinase signaling. *Toxicol. Appl. Pharmacol.* 196, 47–57.
- Kumar, A., Khushboo, Pandey, R., Sharma, B., 2020. Modulation of superoxide dismutase activity by mercury, lead, and arsenic. *Biol. Trace Elem. Res.* 196, 654–661.
- Li, X., Pan, J., Wei, Y., Ni, L., Xu, B., Deng, Y., Yang, T., Liu, W., 2021. Mechanisms of oxidative stress in methylmercury-induced neurodevelopmental toxicity. *Neurotoxicology* 85, 33–46.
- Liao, Y., Peng, S., He, L., Wang, Y., Li, Y., Ma, D., Wang, Y., Sun, L., Zheng, H., Yang, W., Dai, F., Zhao, J., 2021. Methylmercury cytotoxicity and possible mechanisms in human trophoblastic HTR-8/SVneo cells. *Ecotoxicol. Environ. Saf.* 207, 111520.
- Lohren, H., Blagojevic, L., Fitkau, R., Ebert, F., Schildknecht, S., Leist, M., Schwerdtle, T., 2015. Toxicity of organic and inorganic mercury species in differentiated human neurons and human astrocytes. *J. Trace Elem. Med. Biol.* 32, 200–208.
- Lohren, H., Bornhorst, J., Fitkau, R., Pohl, G., Galla, H.J., Schwerdtle, T., 2016. Effects on and transfer across the blood-brain barrier in vitro-Comparison of organic and inorganic mercury species. *BMC Pharmacol Toxicol* 17, 63.
- McCabe, M.J., Eckles, K.G., Langdon, M., Clarkson, T.W., Whitekus, M.J., Rosenspire, A. J., 2005. Attenuation of CD95-induced apoptosis by inorganic mercury: caspase-3 is not a direct target of low levels of Hg<sub>2+</sub>. *Toxicol. Lett.* 155, 161–170.
- Michaelis, V., Aengenheister, L., Tuchtenhagen, M., Rinklebe, J., Ebert, F., Schwerdtle, T., Buerki-Thurnherr, T., Bornhorst, J., 2022. Differences and interactions in placental manganese and iron transfer across an in vitro model of human villous trophoblasts. *Int. J. Mol. Sci.* 23.
- Michaelis, V., Kasper, S., Napierkowski, L., Pusse, J., Thiel, A., Ebert, F., Aschner, M., Schwerdtle, T., Haase, H., Bornhorst, J., 2023. The impact of zinc on manganese bioavailability and cytotoxicity in HepG2 cells. *Mol. Nutr. Food Res.* 67, e2200283.

- Molina-Mesa, S., Martínez-Cendán, J.P., Moyano-Rubiales, D., Cubillas-Rodríguez, I., Molina-García, J., González-Mesa, E., 2022. Detection of relevant heavy metal concentrations in human placental tissue: relationship between the concentrations of Hg, as, Pb and Cd and the diet of the pregnant woman. *Int. J. Environ. Res. Publ. Health* 19, 14731.
- Nesci, S., Trombetti, F., Pirini, M., Ventrella, V., Pagliarani, A., 2016. Mercury and protein thiols: stimulation of mitochondrial F(1)F(O)-ATPase and inhibition of respiration. *Chem. Biol. Interact.* 260, 42–49.
- Novo, J.P., Martins, B., Raposo, R.S., Pereira, F.C., Oriá, R.B., Malva, J.O., Fontes-Ribeiro, C., 2021. Cellular and molecular mechanisms mediating methylmercury neurotoxicity and neuroinflammation. *Int. J. Mol. Sci.* 22, 3101.
- Oliveira, C.S., Joshee, L., Zalups, R.K., Pereira, M.E., Bridges, C.C., 2015. Disposition of inorganic mercury in pregnant rats and their offspring. *Toxicology* 335, 62–71.
- Oliveira, E.M., Rocha, J.B., Sarkis, J.J., 1994. In vitro and in vivo effects of HgCl<sub>2</sub> on synaptosomal ATP diphosphohydrolase (EC 3.6.1.5) from cerebral cortex of developing rats. *Arch. Int. Physiol. Biochim. Biophys.* 102, 251–254.
- Paletz, E.M., Craig-Schmidt, M.C., Newland, M.C., 2006. Gestational exposure to methylmercury and n-3 fatty acids: effects on high- and low-rate operant behavior in adulthood. *Neurotoxicol. Teratol.* 28, 59–73.
- Palomar, A., Quiñero, A., Medina-Laver, Y., Gonzalez-Martin, R., Pérez-Deben, S., Alama, P., Domínguez, F., 2023. Antioxidant supplementation alleviates mercury-induced cytotoxicity and restores the implantation-related functions of primary human endometrial cells. *Int. J. Mol. Sci.* 24.
- Park, J.D., Zheng, W., 2012. Human exposure and health effects of inorganic and elemental mercury. *J. Prev. Med. Public Health* 45, 344–352.
- Pirrone, N., Cinnirella, S., Feng, X., Finkelman, R.B., Friedli, H.R., Leaner, J., Mason, R., Mukherjee, A.B., Stracher, G.B., Streets, D.G., Telmer, K., 2010. Global mercury emissions to the atmosphere from anthropogenic and natural sources. *Atmos. Chem. Phys.* 10, 5951–5964.
- Rand, M.D., Caito, S.W., 2019. Variation in the biological half-life of methylmercury in humans: methods, measurements and meaning. *Biochim. Biophys. Acta Gen. Subj.* 1863, 129301.
- Rodríguez-Viso, P., Domene, A., Vélez, D., Devesa, V., Monedero, V., Zúñiga, M., 2022. Mercury toxic effects on the intestinal mucosa assayed on a bicameral in vitro model: possible role of inflammatory response and oxidative stress. *Food Chem. Toxicol.* 166, 113224.
- Rodríguez-Viso, P., Domene, A., Vélez, D., Devesa, V., Monedero, V., Zúñiga, M., 2023. Oral exposure to inorganic mercury or methylmercury elicits distinct pro-inflammatory and pro-oxidant intestinal responses in a mouse model system. *Food Chem. Toxicol.* 177, 113801.
- Schwarz, M., Löser, A., Cheng, Q., Wichmann-Costaganna, M., Schädel, P., Werz, O., Arnér, E.S.J., Kipp, A.P., 2023. Side-by-side comparison of recombinant human glutathione peroxidases identifies overlapping substrate specificities for soluble hydroperoxides. *Redox Biol.* 59, 102593.
- Shimojo, N., Kumagai, Y., Nagafune, J., 2002. Difference between kidney and liver in decreased manganese superoxide dismutase activity caused by exposure of mice to mercuric chloride. *Arch. Toxicol.* 76, 383–387.
- Smith, P.K., Krohn, R.I., Hermanson, G.T., Mallia, A.K., Gartner, F.H., Provenzano, M.D., Fujimoto, E.K., Goeke, N.M., Olson, B.J., Klenk, D.C., 1985. Measurement of protein using bicinchoninic acid. *Anal. Biochem.* 150, 76–85.
- Tetro, N., Moushaev, S., Rubinchik-Stern, M., Eyal, S., 2018. The placental barrier: the gate and the fate in drug distribution. *Pharm. Res. (N. Y.)* 35, 71.
- Thiel, A., Weishaupt, A.K., Nicolai, M.M., Lossow, K., Kipp, A.P., Schwerdtle, T., Bornhorst, J., 2023. Simultaneous quantitation of oxidized and reduced glutathione via LC-MS/MS to study the redox state and drug-mediated modulation in cells, worms and animal tissue. *J. Chromatogr. B Analyt. Technol. Biomed. Life Sci.* 1225, 123742.
- Tinkov, A.A., Skalnaya, M.G., Demidov, V.A., Serebryansky, E.P., Nikonov, A.A., Skalny, A.V., 2014. Hair mercury association with selenium, serum lipid spectrum, and gamma-glutamyl transferase activity in adults. *Biol. Trace Elem. Res.* 161, 255–262.
- Vázquez, M., Vélez, D., Devesa, V., 2014. In vitro evaluation of inorganic mercury and methylmercury effects on the intestinal epithelium permeability. *Food Chem. Toxicol.* 74, 349–359.
- Wallace, D., 2015. Differential effects of organic and inorganic mercury on phenotypically variant breast cancer cell lines. *J. Clin. Toxicol.* (5).
- Wang, Y., Walsh, S.W., 2001. Increased superoxide generation is associated with decreased superoxide dismutase activity and mRNA expression in placental trophoblast cells in pre-eclampsia. *Placenta* 22, 206–212.
- WHO, 2017. **Mercury and Health**. <https://www.who.int/news-room/fact-sheets/detail/mercury-and-health>.
- Yang, L., Zhang, Y., Wang, F., Luo, Z., Guo, S., Strähle, U., 2020. Toxicity of mercury: Molecular evidence. *Chemosphere* 245, 125586.
- Ye, K., Chen, Z., Xu, Y., 2023. The double-edged functions of necroptosis. *Cell Death Dis.* 14, 163.
- Zalups, R.K., 2000. Molecular interactions with mercury in the kidney. *Pharmacol. Rev.* 52, 113–143.
- Zharova, T.V., Grivennikova, V.G., Borisov, V.B., 2023. F1-Fo ATP synthase/ATPase: contemporary view on unidirectional catalysis. *Int. J. Mol. Sci.* 24, 5417.